PNAS

Size, Shape, and the Thermal Niche of Endotherms
Author(s): Warren P. Porter and Michael Kearney
Source: *Proceedings of the National Academy of Sciences of the United States of America*,
Vol. 106, Supplement 2: Biogeography, Changing Climates, and Niche Evolution (Nov. 17,
2009), pp. 19666-19672
Published by: National Academy of Sciences
Stable URL: http://www.jstor.org/stable/25593252
Accessed: 15-09-2016 17:49 UTC

REFERENCES

Linked references are available on JSTOR for this article:
http://www.jstor.org/stable/25593252?seq=1&cid=pdf-reference#references_tab_contents
You may need to log in to JSTOR to access the linked references.

National Academy of Sciences is collaborating with JSTOR to digitize, preserve and extend access to
Proceedings of the National Academy of Sciences of the United States of America

Size, shape, and the thermal niche of endotherms

Warren P. Porter[a,1] and Michael Kearney[b]

[a]Department of Zoology, University of Wisconsin, Madison, WI 53706; and [b]Department of Zoology, University of Melbourne, Victoria 3010, Australia

A key challenge in ecology is to define species' niches on the basis of functional traits. Size and shape are important determinants of a species' niche but their causal role is often difficult to interpret. For endotherms, size and shape define the thermal niche through their interaction with core temperature, insulation, and environmental conditions, determining the thermoneutral zone (TNZ) where energy and water costs are minimized. Laboratory measures of metabolic rate used to describe TNZs cannot be generalized to infer the capacity for terrestrial animals to find their TNZ in complex natural environments. Here, we derive an analytical model of the thermal niche of an ellipsoid furred endotherm that accurately predicts field and laboratory data. We use the model to illustrate the relative importance of size and shape on the location of the TNZ under different environmental conditions. The interaction between body shape and posture strongly influences the location of the TNZ and the expected scaling of metabolic rate with size at constant temperature. We demonstrate that the latter relationship has a slope of approximately ½ rather than the commonly expected surface area/volume scaling of ⅔. We show how such functional traits models can be integrated with spatial environmental datasets to calculate null expectations for body size clines from a thermal perspective, aiding mechanistic interpretation of empirical clines such as Bergmann's Rule. The combination of spatially explicit data with biophysical models of heat exchange provides a powerful means for studying the thermal niches of endotherms across climatic gradients.

biophysical ecology | functional traits | lower critical temperature |
metabolic scaling | thermoneutral zone

The ecological niche reflects the interaction between an organism and its environment and how that interaction affects its fitness (1, 2). An understanding of a species' niche requires knowledge of its traits (morphology, physiology, and behavior) and how that species interacts with its habitat to construct environments (2). This two-way interaction between organism and environment is also key to understanding how a species' traits, and hence its niche, evolves (3, 4). A species' energy and water balance are key determinants of its niche, reflecting both its requirements for life (Grinnellian niche) and its impact on the other species with which it interacts (Eltonian niche). Here, we illustrate how biophysical principles can be used to link variation in the size, shape, and other functional traits of organisms with environmental data to predict the thermal niches of endotherms. Such a model can be conceived as a mechanistic depiction of the Hutchinsonian niche, a hypervolume describing conditions suitable for survival, growth, and reproduction along trait and environmental axes. Biophysical models provide a way to calculate spatially explicit null models of selective pressures on functional traits from the perspectives of energy and water conservation (5).

Basal metabolic rate (BMR), the lower bound on the metabolic rate of nontorpid endotherms, scales very predictably with body mass as a power function with an exponent of ≈3/4. Although the underlying basis for this scaling relationship remains controversial (6–8), its generality can be used to explain many ecological patterns (9). Yet BMR measures determined under standardized animal and laboratory conditions provide only limited insight into the energy and water exchange of animals in natural environments. They only tell us what the energy requirements would be if the animal could find an environment permitting a BMR; such measures say nothing about the difficulty of reaching basal rates in a given location, nor can they tell us the consequences of failing to reach basal rates.

BMR is estimated by using fasted, resting animals measured under a range of environments. Below a particular value of air temperature, the lower critical temperature (LCT), metabolic rate rises above the BMR to maintain a constant core temperature (Fig. 1). Increases in air temperature above the LCT eventually cause the metabolic rate to rise once more with a concomitant rapid increase in water loss rate as the animal attempts to dump excess heat to its environment. The "comfort zone" where animals can reach their BMR without enhanced water loss is known as the thermoneutral zone (TNZ) (10). It is the capacity to be within the TNZ, and the consequences of being outside it, that we must understand to estimate energy and water budgets in nature. Empirical studies of the TNZ are local descriptions contingent on the particular combinations of air temperature, wind speed, radiation, and humidity used in the experiment, fur properties, size, and shape. Statistical descriptions derived from them cannot be used to generalize TNZs in other environments (11, 12). Instead, we need a mechanistic approach to understand how evolutionary changes in key traits such as size and shape relate to energy and water costs across natural environmental gradients.

Here, we derive a geometric model of the thermal dependence of metabolic rate for ellipsoidal, furred endothermic organisms as a function of the radiative and convective environment. Previous models of distributed heat generation in an endotherm heat balance either require numerical solution or are restricted to perfect spheres. The ellipsoid model (Dataset 1) we present provides an analytical solution that allows a more representative basis for endotherm shapes than previous models based on cylinders or slabs and represents the only truly 3D heat flux solution with distributed heat generation other than that for spheres. The ellipsoid model is also useful in the present context because it allows variation in shape that mimics what occurs in animals. We use this model to explore the impact of changes in shape, size, fur depth, and environmental conditions on the location of the TNZ. We show, using the brush-tail possum of Australia, how this approach can be combined with data on environmental gradients to generate null models of spatial clines in body size and shape such as Bergmann's Rule and Allen's Rule.
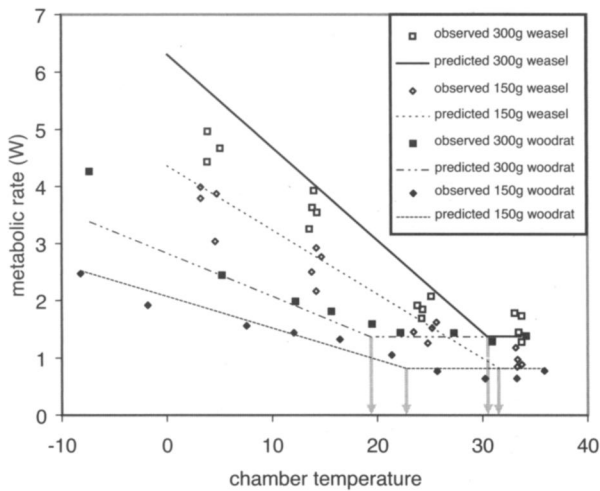
Fig. 1. Observed metabolic rates as a function chamber temperature in laboratory studies of the weasel and the woodrat by Brown and Lasiewski (20) together with predicted values based on an analytical biophysical model of convective and radiant heat exchange in a furred ellipsoid with distributed heat generation using the parameters in Table 1. Light gray arrows indicate the location of the LCT and hence the beginning of the TNZ.

Results and Discussion

Calculating TNZs from First Principles. BMRs and TNZs are typically measured in metabolic chambers where the dominant processes of heat exchange are convection, Q_{conv}, metabolism, Q_{gen} and thermal infrared radiation, Q_{IR} (13). If we assume a chamber emissivity of near one, the simplest possible geometric model of heat exchange for furred ellipsoid endotherms $Q_{gen} = Q_{conv} + Q_{IR}$ is

$$Q_{gen} = \left[\frac{(T_c - T_f)}{\dfrac{S^2}{2k_b V_b} + \dfrac{b_o - b}{4\pi b b_o k_{ins}} + \dfrac{R_{cv} R_{rad}}{R_{cv} + R_{rad}}} \right]. \qquad [1]$$

Eq. 1 is derived in *SI Appendix*. The gradient between core and fluid temperatures, T_c and T_f, is divided by the total thermal "resistance" consisting of three resistances that are a consequence of the geometry of the animal and the distributed heat generation. Eq. 1 is in contrast to a central point source and slab or cylinder geometry equation, which is typically used. The first resistance term is for the body with distributed heat generation, the second is for the furry insulation, and the third is the equivalent resistance for convective and thermal infrared radiant heat exchange with the environment. The first spheroid resistance contains variables with units of area, volume, and thermal conductivity: S^2, V_b, and k_b. S^2 is a shape factor of the ellipsoid's semimajor (a) and semiminor (b, c) axes (see below), V_b is the body volume, and k_b is the effective thermal conductivity of the body. The second spheroid resistance consists of b, the body semiminor axis, b_o, the body plus fur semiminor axis, and k_{ins}, the effective thermal conductivity of the porous fur insulation. The third spheroid resistance describes the parallel resistances to convective, R_{cv}, and radiant, R_{rad}, heat exchange. The convection and radiation resistances are complex and contain properties of the animal and the environment around it. The full derivation and definition of all of the terms in these equations can be found in *SI Appendix*.

From these considerations, we can state that the heat generation requirement, Q_{gen}, that is consistent with maintaining any desired core temperature given the current environmental conditions, depends on the body characteristic dimension L, taken here to be the cube root of the volume (14), the area A, the body

volume V_b, the temperature-dependent fluid properties (air in this case), i.e., density ρ, dynamic viscosity μ, specific heat c_p, velocity v, the temperatures of the core T_c and fluid T_f, the effective radiant temperature of the environment in Kelvin, the emissivity of the animal, which is typically close to 1.0, the effective thermal conductivities of the body k_b, the insulation k_{ins}, the fluid thermal conductivity k_f, and the animal's geometric shape factor S^2. For an ellipsoid, this shape factor is

$$S^2 = \frac{a^2 b^2 c^2}{a^2 b^2 + a^2 c^2 + b^2 c^2}, \qquad [2]$$

where a, b, and c are the semimajor and minor axes of the ellipsoidal body and a_o, b_o, and c_o in Eq. 1 are the semimajor and minor axes at the tips of the body's insulation.

The relationship between core and skin temperature for an ellipsoid without insulation is

$$T_c - T_s = \frac{q'''}{2k_b} \left[\frac{a^2 b^2 c^2}{a^2 b^2 + a^2 c^2 + b^2 c^2} \right]. \qquad [3]$$

(15), where q''' is the heat generation per unit volume and T_s is skin temperature.

We typically compute the total heat generation by solving Eq. 1 using the morphological, physiological, and environmental properties described above and in *SI Appendix*. However, in this article we also turn this concept around and use the experimentally determined minimum (resting) metabolic rate and solve for the air temperature consistent with the measured BMR and known environmental (chamber or outdoor) variables that also simultaneously affect the core temperature. In this way, we can find the lower critical air temperature (16), i.e., the low-temperature end of the TNZ, by solving Eq. 1 for air temperature using minimum allowable metabolic rate of nontorpid mammals (or birds), i.e., the mouse to elephant curve (17). Eq. 1 specifies requisite data that should be collected to extrapolate chamber measurements of metabolic rates to environments outside the experimental apparatus.

Shape Effects on the Thermal Niche: Weasels and Woodrats in Metabolic Chambers. Empirical measures of the TNZ are clearly local analyses that cannot be generalized to other environmental conditions (11) without a complete set of data defined in Eq. 1. We can, however, compute the TNZ from first principles as we have described above. This allows us to produce quantitative answers to a wide range of questions about the influence of functional trait variation on the thermal niche of an endotherm.

From the considerations above it is clear that animals of the same volume but of different shape should reach their TNZ at different metabolic chamber temperatures (16). Although a number of studies have considered the influence of shape on metabolic rate (e.g., refs. 12, 18, and 19) the only study we are aware of that explicitly examined combined effects of size and shape on the TNZ of endotherms in metabolic chambers was the pioneering work on weasels and woodrats by Brown and Lasiewski (20). Predictions from our analytical model, using the parameters in Table 1 (see *Materials and Methods*), compare closely with their empirical data (20) (Fig. 1). The lower core body temperature and more spherical shape of the woodrat contributed to it reaching its TNZ at a much lower air temperature than did the weasel. The effect of shape on the TNZ, holding core temperature, and volume constant at that of the 150-g female weasel, is shown in Fig. 2A. The LCT shifts by >7.0 °C as the length/width ratio changes from 1.5 to 5.5. However, chamber wind speed also influences the TNZ (Fig. 2B), as does humidity and the thermal radiative environment. Increasing the wind speed in the chamber an order of magnitude above the approximate speed used in the empirical analysis

Table 1. Parameter estimates used to model empirical data on the thermal dependence of metabolic rate in a variety of mammals

Species	Body weight, kg	Body dimensions ratio a:b = c	Body thermal conductivity, W/m-°C	Fur depth, mm	Fur conductivity, W/m-°C	Core temperature, °C	Wind speed, mm/s	Predicted lower critical temperature, °C	Ref.
Longtail weasel	0.150	2.6	0.5	5.3	0.0272	39	0.67	31.6	20
	0.300	2.6	0.5	5.3	0.0272	39	0.74	30.5	20
Woodrat	0.151	1.6	0.5	13.9	0.0365	37.3	0.82	22.7	20
	0.299	1.6	0.5	13.9	0.0365	37.6	1.04	19.3	20
White fox	4.65	1.5	0.5	49.8	0.0272	37.0	1.0	−27.4	23, 24
Northern collared lemming	0.055	1.5	0.5	19.3	0.0272	37.0	1.0	25.2	23, 24
Eskimo dog pups	12.0	1.5	0.5	40.7	0.0272	37.0	1.0	−39.8	23, 24
Polar bear cubs	8.9	4.5	0.5	44.3	0.0272	37.0	1.0	5.3	23, 24
Ground squirrel	1.1	1.5	0.5	14.4	0.0272	37.0	1.0	10.4	23, 24
Least weasel	0.05	1.5	0.5	7.4	0.0272	37.0	1.0	27.2	23, 24
White-nosed coati	4.15	4.5	0.5	13.25	0.0272	37.0	1.0	22.9	23, 24
Jungle rat	0.265	1.5	0.5	7.3	0.0272	37.0	1.0	22.5	23, 24
Marmoset	0.225	1.5	0.5	12.76	0.0272	37.0	1.0	19.7	23, 24
Night monkey	0.82	4.5	0.5	17.3	0.0272	37.0	1.0	25.6	23, 24
Crab-eating raccoon	1.16	4.5	0.5	7.3	0.0272	37.0	1.0	28.9	23, 24
Two-toed sloth	3.8	4.5	0.5	35.0	0.0272	37.0	1.0	27.2	23, 24
Brushtail possum	2.5	1.5	0.5	17.0	0.0272	36.2	222	12.4	49, 50

(0.0005 to 0.005 ms^{-1}) had an indistinguishable effect on the TNZ of the weasel, but further increases up to 5 ms^{-1} had as much as a 1.5 °C impact (Fig. 2B) (note that our model does not include the effect of high wind speeds on compressing or disrupting the fur layer). Although weasels are an extreme case, important shape variation is present in endotherms (21) that can, of course, be modified strongly by posture. Unfortunately,
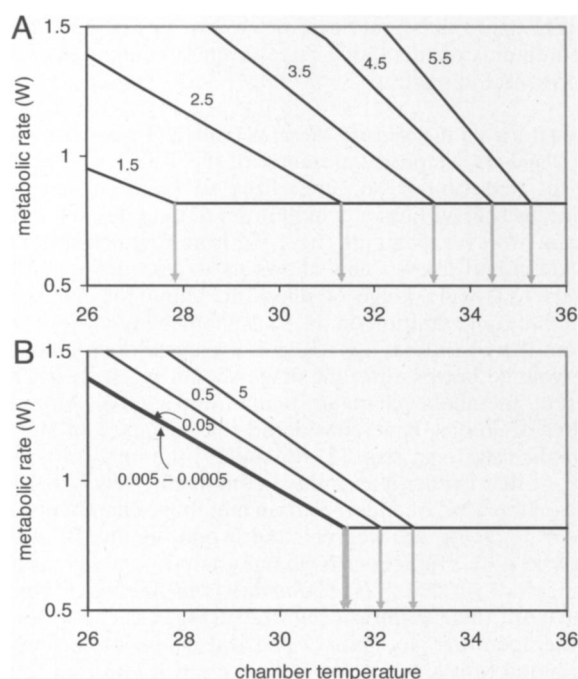

Fig. 2. The simulated effect of variation in posture (A) and wind speed (B) on the TNZ of a 150-g weasel. In postural analyses, shape was allowed to vary according to changes in the ratios of the semimajor axes a and b of between 1.5 and 5.5, assuming an oblate spheroid with fur of depth 5.3 mm, holding wind speed constant at 0.7 mm/s. For wind speed analyses, wind speed was varied by orders of magnitude from 0.5 mm/s to 5 m/s, holding shape constant at a 2.5 ratio between the semimajor axes a and b. Light gray arrows indicate the location of the LCT and hence the beginning of the TNZ.

posture and local wind speed experienced by the animal are rarely recorded or reported in any detail in metabolic chamber studies, despite their significance to the location of the lower critical temperature.

Size Effects on the Thermal Niche: Mice to Elephants. We now use our analytical model to illustrate the interactive influences of body size and shape on required metabolic heat generation and the location of the TNZ. To illustrate this we first calculated metabolic rate as a function of size and shape across a range of body sizes representing mice to elephants at constant air temperature (Fig. 3). We considered two different length/width ratios, a sphere and a prolate ellipsoid with a:b = c of 5:1, and used dimensionless Nusselt-Reynolds correlations for spheres (14, 22) to calculate heat transfer by these bodies for different wind speeds at an air temperature of 20 °C. It is often stated that the BMR of endotherms was originally expected to scale with mass to the power of 2/3 because of Euclidian arguments about the way surface area scales with volume. In contrast, our analyses predict different slopes depending on the shape of the organism, the wind speed and its insulation properties, with values consistently <2/3. This slope difference occurs in part because the temperature of a living endotherm is not uniform, but rather develops a temperature gradient from core to skin that increases in magnitude nonlinearly with increasing body axes sizes (Eq. 3). Moreover, blood flow varies with size and with it the effective conductivity of the body (see *SI Appendix*). Pelt depth and the associated resistance of the fur may also vary in a complex manner with size. These internal resistances further reduce the required heat generation to maintain a constant core temperature from that expected from simple considerations of surface area-to-volume ratios. All of these processes are minimized in the case of a spherical copper (high thermal conductivity reduces internal thermal resistance) object with no hair, which has a slope closest to the expected 2/3 (Fig. 3). Finally, under forced convection, boundary layer thickness also increases with size that also increases the resistance of larger organisms, especially those without fur (Fig. 3B).

Note that the calculations presented in Fig. 3 do not represent the expected slope of the relationship between BMR and body mass, famously shown by Kleiber to be ¾. Kleiber's law is a reflection of cellular and physiological constraints (8, 23) and is
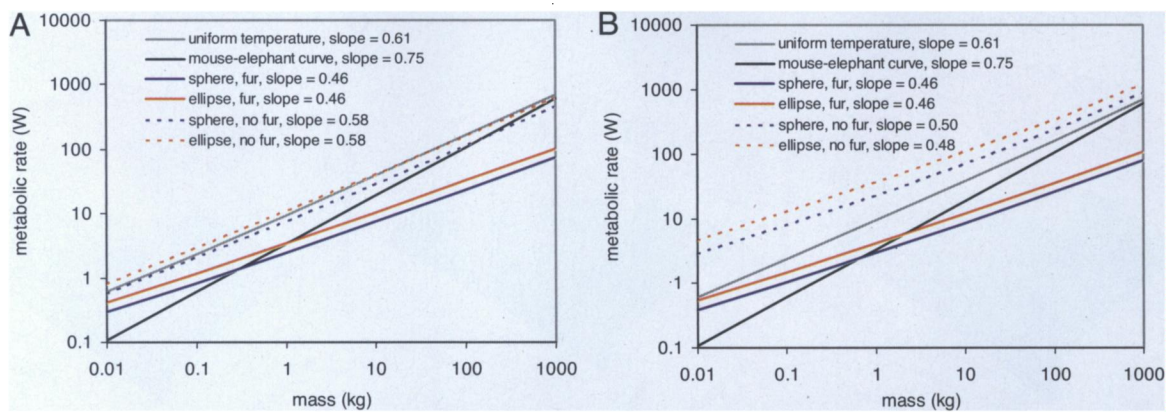
Fig. 3. The effect of size, shape (sphere vs. ellipsoid with a:b = c 5:1), and pelage on the metabolic rate at constant air temperature, 20 °C, under low wind speed as found in metabolic chambers (0.001 m/s) (*A*) and high wind speed (10 m/s) (*B*). Calculations are based on the ellipsoid model as described. Also indicated on each graph are the mouse–elephant empirical relationship for BMR and the expected relationship for a copper sphere. Where predicted metabolic rate goes below the mouse–elephant curve, animals would be above their LCT and may have to lose considerable heat through evaporation or enhanced blood flow to specialized appendages (e.g., elephant ears) to maintain constant core. Note that the slope of the relationship between metabolic rate and body mass is considerably lower than expected from simple considerations of surface area/volume unless the organism is of uniform temperature, as is the case for copper sphere.

obtained by adjusting an endotherm's environmental conditions during measurement until a basal level is reached (the cold end of the TNZ). Thus, environmental conditions are not consistent across the extent of the mouse to elephant curve.

Combined Influences of Size, Shape, and Fur on the TNZ. Figs. 3 and 4 suggest that there may be functional constraints on the ratio of body length to body width as animals change in mass. However, the effects of these traits are also mediated by the powerful
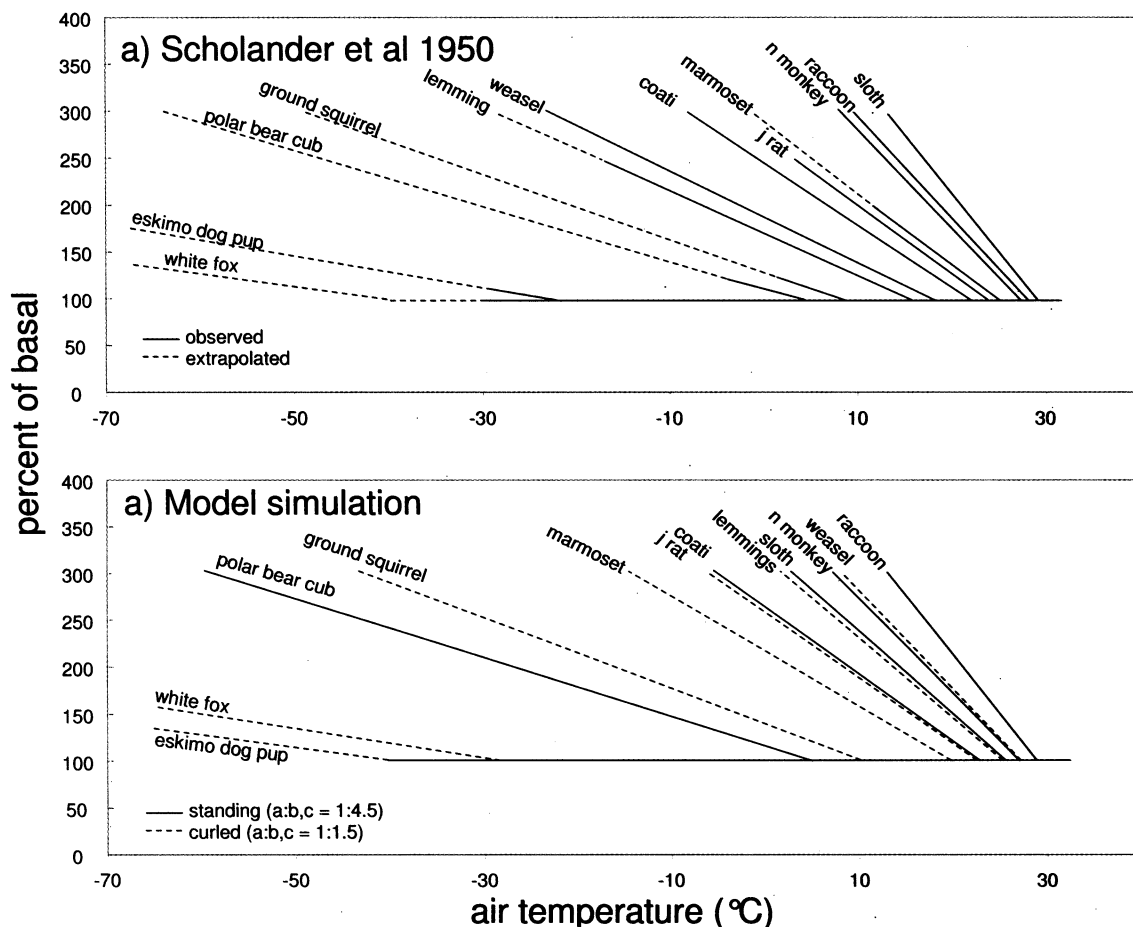

Fig. 4. Metabolic rate relative to basal as a function of air temperature for a variety of mammals as measured in environmental chambers by Scholander et al. (24) (*A*) and as predicted by our analytical ellipsoid model of heat exchange in a furred endotherm (*B*) (see also Fig. S2). Parameter values are presented in Table 1.
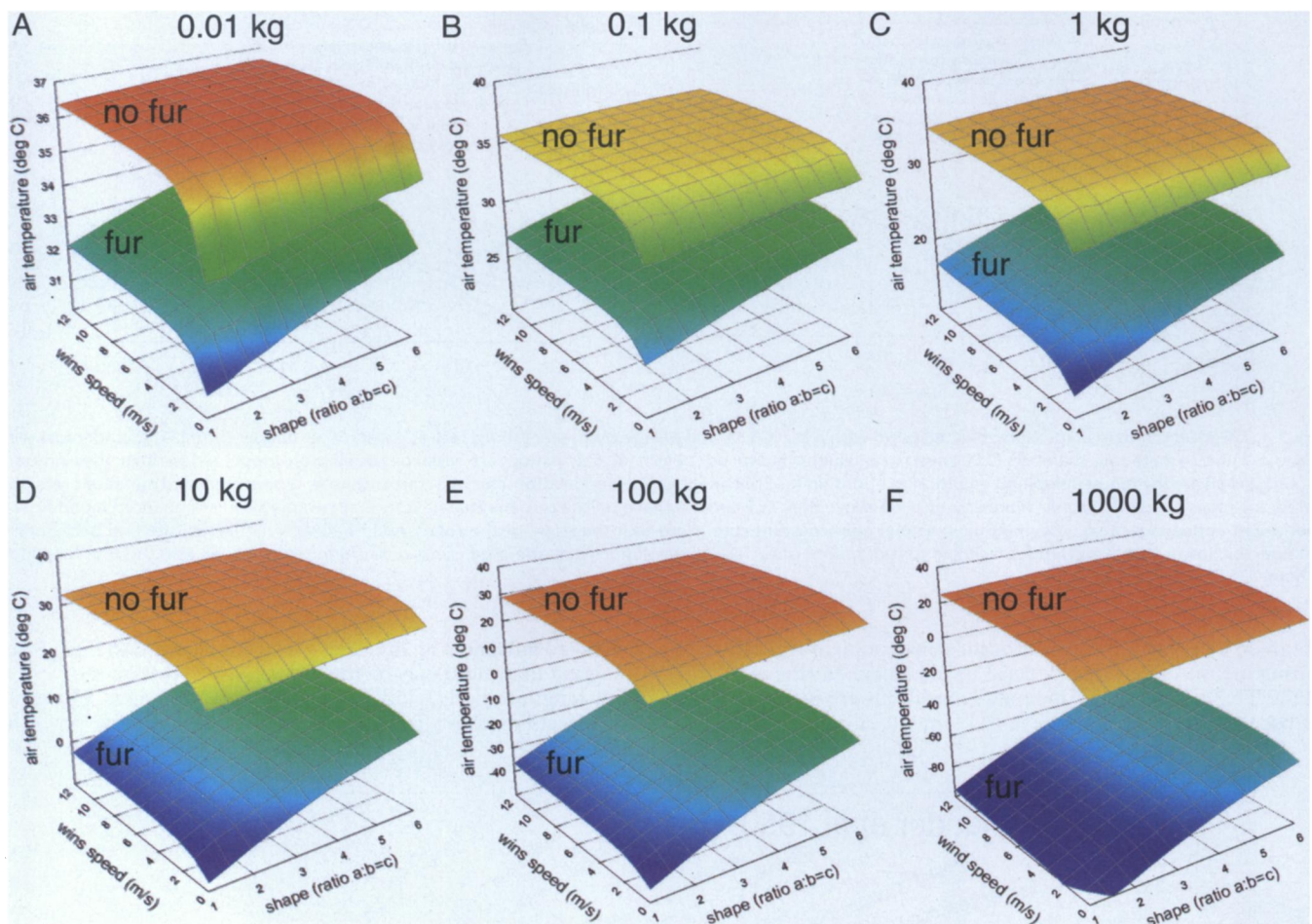
Porter and Kearney

Fig. 5. Simulated lower critical air temperature (beginning of the TNZ) for different size endotherms as a function of posture and wind speed. Results are presented for animals with and without fur. Notice that smaller animals have much stronger response to lower wind speeds than larger animals because of their thinner boundary layer thickness and hence stronger coupling to air temperature effects.

thermal resistance of the pelage (16). Scholander et al. (24, 25) provided an extensive dataset on the LCTs of a wide range of mammalian taxa ranging in size from 0.05 to 12 kg (Fig. 4A), with small animals such as the white fox (4.5 kg) obtaining LCTs well below −20 °C as a result of their fur properties. Our ellipsoid model predicts that, across all sizes and shapes considered in Fig. 3, the fur insulation resistance, R_{ins}, accounts for ≈60–88% of the total resistance to heat transfer ($R_T = R_b + R_{ins} + R_E$) (see *SI Appendix*). However, as body size increases, the absolute magnitude of the value of the R_T drops from values of ≈10 for the 10-g body sizes to absolute values of ≈0.01 for the very largest animals (10^4 kg). Thus, it suggests that differences in fur depth have the greatest impact for animals of small size.

We can rearrange Eq. **1** to solve for the fluid temperature that would result in the empirically observed BMR. It allows us to determine the combinations of wind speeds, air temperatures, and shapes that would permit an endotherm to be within its TNZ at different body sizes. We reconstructed Scholander et al.'s (24) figure from first principles by using this approach, with comparable results (Fig. 4B), depending on the posture used in the analysis (Fig. S1) (not reported in the original study). The only major deviations of our model from the empirical data were for the northern collared lemming and the least weasel, which required core body temperatures lower than those reported (25) for a close match (32 °C vs. 37 °C).

We can generalize these analyses to a broader range of body

sizes and depict the TNZ in linear climate space diagrams bounding the lower and upper critical temperatures (Fig. 5). Climate space is typically considered in the four dimensions of air temperature, wind speed, radiation, and humidity (26). However, the inclusion of a morphometric axis in the climate space diagrams in Fig. 5 emphasizes how the thermal niche of an organism is the result of interactions between physical conditions and functional traits such as posture and shape (27). It can be seen in Fig. 5 that as size increases (or fur insulation decreases) there is a dramatic increase in the width of the TNZ and a shift downward. Note that in these analyses the upper critical temperature was estimated as the coolest environment permitting BMR when blood flow to the skin is maximized (see *Materials and Methods*). It is therefore an underestimate because considerable heat is lost by evaporation through normal respiration and, in some organisms, heat is lost via blood flow through specialized structures, such as the ears of African elephants (28).

Thermal Niches Across Environmental Gradients in Nature. Endotherms in nature are exposed to daily and seasonal variation in air temperature, wind speed, solar radiation, and humidity, all of which influence energy and water costs (12). Animals also have the capacity to behaviorally select suitable microenvironments within their habitat. A mechanistic model of these processes, when combined with spatial data on climate, provides a means to ask how functional traits might be expected to vary under
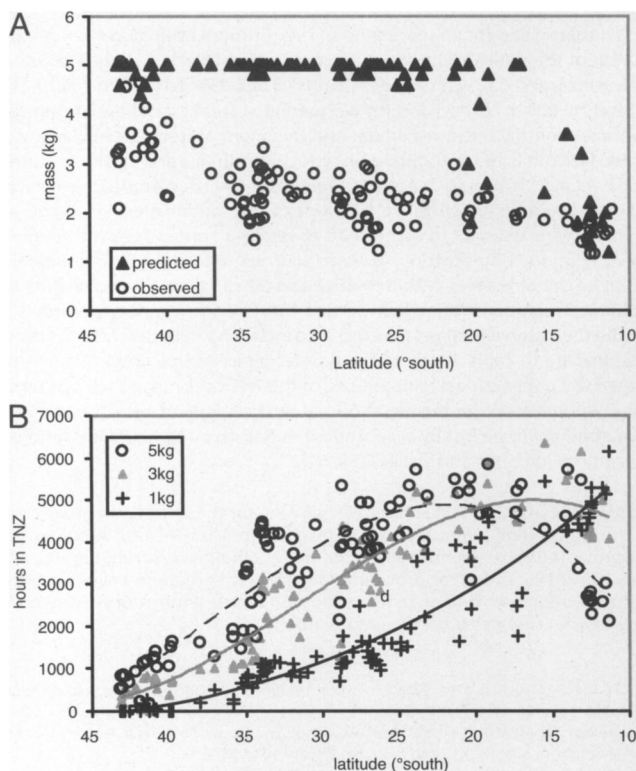
Fig. 6. Analysis of a Bergmann's cline in the Australian brush-tail possum (*Trichosurus vulpecula*) using the furred ellipsoid model (see Table 1 for parameter values). (*A*) The observed Bergmann's cline (from ref. 37) compared with the expected cline that would maximize time spent within the TNZ. (*B*) Latitudinal change in the predicted time within the TNZ for three different body sizes.

different selection regimes across environmental gradients. For instance, we may ask which body size within a specified range maximizes time spent within the TNZ. Such analyses are critical for understanding ecological patterns at the level of the community (29, 30).

Body size is observed to increase in many endothermic taxa as temperature decreases, a phenomenon known as Bergmann's Rule (31–34). A major explanation for Bergmann's clines in body size is based on energetic and hydric considerations (35, 36). Yet body size is the end result of a tug of war of a great many selective forces, and there are numerous alternative explanations and expectations for body size clines that are not mutually exclusive (16, 35). Efforts to distinguish among explanations for Bergmann's clines often involve comparisons of the relative strength of correlations between size and distal environmental variables such as latitude and mean annual temperature (34, 37). Biophysical principles, however, allow one to derive more proximal variables that reflect the interaction between organism and environment and can be tailored more specifically to individual species.

To illustrate this, we have applied our analytical ellipsoid model to derive an expected latitudinal size cline in the Australian brush-tailed possum, which shows a classic Bergmann's cline (37) (Fig. 6*A*). The present model, which considers only convective and thermal infrared radiative exchange, is appropriate for this nocturnal, cavity dwelling species if we can assume that it spends most of its time in deep shade (thereby approximating blackbody environmental conditions). Our model compares extremely well with field measures of metabolic rate when solar radiation is absent (Table S1 and Fig. S2). More detailed,

computationally intensive approaches can be applied in more complex environmental settings (15, 38, 39).

We used the furry ellipsoid model to derive the expected cline if selection has favored, in each location, the body size that maximizes the annual hours spent within the TNZ, allowing mass to take any value from 1 to 5 kg at 0.2-kg intervals (Fig. 6*A*) (see *Materials and Methods*). Note that by focusing on time spent within the TNZ we are not basing selection on a mass-specific basis (see ref. 40). The result is in good quantitative agreement with the observed body size cline at latitudes below ≈20°, where hours within the TNZ start to decline for the 5-kg animals relative to smaller animals (Fig. 6*B*) because the larger animals begin to experience environments above the thermal neutral zone (heat stress). However, at latitudes >20° latitude, 5 kg almost always optimizes time within the TNZ (Fig. 6 *A* and *B*), whereas observed body size clines much more gradually. Thus, despite a qualitatively similar prediction for larger body size toward the poles, our analysis reveals quantitative discrepancies between the observed data and our hypothesized selective force. This analysis could be extended in many ways, for instance by incorporating weather extremes, energy and water budgets that account for diet and feeding rates, retreat-site heat exchange, and the effects of gene flow. The point is that the application of a mechanistic, functional trait-based model of the thermal niche of endotherms allows the construction of quantitative hypotheses for expected clines under different scenarios.

Conclusions

The principles of biophysical ecology provide a powerful means for studying the thermal niches of endotherms. Despite the capacity of endotherms to maintain fixed core temperatures in a wide range of environments, this core temperature may come with a significant energy or water cost. Thus, endotherms, like ectotherms, can have very restricted thermal niches in terms of the combinations of air temperature, wind speed, radiation, and humidity that permit survival, growth, and reproduction. We have shown how it is possible to calculate the consequences of variation in both environments and functional traits for key aspects of an endotherm's fundamental niche such as the location of the TNZ. When data are available on food availability, feeding rates, and digestive capabilities, one can ask more detailed questions about energy and water balance (39, 41–43). When combined with spatially explicit estimates of environmental conditions, biophysical models provide the opportunity for studying clinal patterns in functional traits such as body size and shape, pelage, color (solar reflectance) and core temperature, and constraints on distribution and abundance (44). This furry ellipsoid model provides a powerful means by which to incorporate environmental gradients into analyses of evolutionary change (5). We hope this study encourages further biophysical explorations of the thermal niches of endotherms. Such studies will enhance our understanding of endothermy as a thermoregulatory strategy and will help us to better anticipate the responses of endotherms to future climate change.

Materials and Methods

Model Validation and Sensitivity Analyses. We tested our model predictions in this article against field and laboratory metabolic measurements of a variety of mammalian taxa (12, 20, 24, 25, 45) (Figs. 1 and 5 and Fig. S2). Parameter estimates (Table 1 and Table S1) came from the aforementioned papers unless otherwise stated. For the comparison against the Brown and Lasiewski (20) data, the weasel was modeled as an oblate spheroid (a disk-like shape, a = b:c 2.6) and the woodrat was modeled as a prolate spheroid (a football-like shape a:b = c 1.6), based on Brown and Lasiewski's observations of resting individuals. All other animals were modeled as prolate spheroids. For comparison against the Chappell (12, 45) data we used ratios for a:b,c of 5 for weasels and 3 for other taxa (Table S1), which provided a good match with observed diameters and surface areas. For comparisons against the Scholander et al. (24, 25) data, no postural data were available and so we used a:b, c ratios of 1.5

Porter and Kearney

(curled) and 4.5 (standing) (Table 1). A key parameter not measured for the individuals used in the Brown and Lasiewski and Scholander et al. studies was the thermal conductivity of the fur. The thermal conductivity of woodrat fur was taken from Webb and McClure (46) and that of weasel fur was taken from Davis and Birkebak (47). Actual fur conductivities can vary among individuals and we note that subtle changes in this parameter (e.g., from 0.027 to 0.022 W/m-C for 300-g weasels) produced an even closer fit to the empirical data than depicted in Fig. 1. We used a value of 0.027 for all other analyses. Local wind speeds in the metabolic chamber used by Brown (48) to measure wood rat metabolic rates were estimated based on volumetric air flow rates of 600 cm³/min in a 1-gallon cylindrical chamber of dimensions 16.2 × 18.7 cm (diameter × height). Wind speeds for the weasel were estimated similarly based on flow rates of 1,500 cm³/min in a 3-gallon cylindrical chamber of inferred dimensions 23.5 × 27.1 cm (diameter × height) (20). Blockage effects by the animals accelerated flow by ≈50% based on their estimated volume and density. For all other analyses we used a flow rate of 1 mm/s.

Sensitivity analyses of the LCT were applied to a broader range of shape, size, wind speeds, and air temperatures than in the tests against empirical data described above. For these theoretical analyses of effects of body size and different length/width ratios we altered fur depth as a function of mass to correct for increasing fur depth with increasing mass. These calculations were based on fur data collected by W.P.P. from 11 species of mammals ranging in size from shrews to elk. The data are described by the regression equation: fur depth (mm) = 9.01 mass (kg)$^{0.165}$ (R^2 = 0.46, t_{15} = 3.59, P = 0.003).

Environmental Gradient Analyses. Analysis of the latitudinal cline in body mass in the brush-tail possum was based on the raw locality and size data (37),

summarized as the maximum observed size per site across all individuals. Mass was not provided for all specimens and was instead estimated from greatest length of the skull (GTL) using a power function fitted to all data points for which mass and GTL was recorded: mass = 3.54E-05 × GTL$^{4.06}$ (R^2 = 0.73, t_{13} = 9.59, P < 0.0001). For each locality we queried a climatic database of long-term average monthly mean maximum and minimum air temperature and wind speed (49) and fitted sinusoidal 24-h cycles with minima and maxima occurring at dawn and 1 h after solar noon (corrected for local day length), respectively. Full shade was assumed for calculations of the radiative environment, and animals were assumed to be perched at weather station height throughout the day in a sitting posture. At each hour we used the ellipsoid model to estimate the time spent within the TNZ and the difference between BMR and predicted metabolic rate when outside the TNZ for a variety of body sizes within the observed range (1–5 kg, 0.2-kg intervals). Parameters for brush-tail possums are in Table 1. The LCT was determined as described. We approximated the upper critical temperature of the TNZ for brush-tailed possums as the environment requiring metabolic rate to be <60% of basal (i.e., >40% of BMR required to be lost by evaporation), based on published observations of thermoregulation in this species (50, 51).

1. Chase JM, Leibold MA (2003) *Ecological Niches* (Univ Chicago Press, Chicago).
2. Kearney M (2006) Habitat, environment, and niche: What are we modeling? *Oikos* 115:186–191.
3. Lewontin RC (2000) *The Triple Helix: Genes, Organism, and Environment* (Harvard Univ Press, Cambridge, MA).
4. Oldling-Smee FJ, Laland KN, Feldman MW (2003) *Niche Construction: The Neglected Process in Evolution* (Princeton Univ Press, Princeton).
5. Kearney M, Porter WP, Williams CK, Ritchie SA, Hoffmann AA (2009) Integrating biophysical models and evolutionary theory to predict climatic impacts on species' ranges: The dengue mosquito *Aedes aegypti* in Australia. *Funct Ecol* 23:528–538.
6. Kozlowski J, Konarzewski M, Gawelczyk AT (2003) Cell size as a link between noncoding DNA and metabolic rate scaling. *Proc Natl Acad Sci USA* 100:14080–14085.
7. van der Meer J (2006) Metabolic theories in ecology. *Trends Ecol Evol* 21:136–140.
8. West GB, Brown JH, Enquist BJ (1997) A general model for the origin of allometric scaling laws in biology. *Science* 276:122–126.
9. Brown JH, Gillooly JF, Allen AP, Savage VM, West GB (2004) Toward a metabolic theory of ecology. *Ecology* 85:1771–1789.
10. Nichelmann M, Tzchentke, B (1995) in *Body Temperature and Metabolism*, eds Nagasaka T, Milton AS (International Press Editing Centre, Inc., Tokyo), pp 77–82.
11. Romanovsky AA, Ivanov AI, Shimansky YP (2002) Selected contribution: Ambient temperature for experiments in rats: A new method for determining the zone of thermal neutrality. *J Appl Physiol* 92:2667–2679.
12. Chappell MA (1980) Thermal energetics and thermoregulatory costs of small Arctic mammals. *J Mammal* 61:278–291.
13. Porter WP (1969) Thermal radiation in metabolic chambers. *Science* 166:115–117.
14. Mitchell JW (1976) Heat transfer from spheres and other animal forms. *Biophys J* 16:561–569.
15. Porter WP, Munger JC, Stewart WE, Budaraju S, Jaeger J (1994) Endotherm energetics: From a scalable individual-based model to ecological applications. *Austral J Zool* 42:125–162.
16. Scholander PF (1955) Evolution of climatic adaptation in homeotherms. *Evolution (Lawrence, Kans)* 9:15–26.
17. Gordon MS, Bartholomew GA, Grinnell AD, Jorgensen CB, White FN (1972) *Animal Physiology: Principles and Adaptations* (Macmillan, New York).
18. Rubsamen K, Hume ID, Foley WJ, Rubsamen U (1984) Implications of the large surface area to body mass ratio on the heat balance of the greater glider (*Petauroides volans*: Marsupialia). *J Comp Physiol B* 154:105–111.
19. Bartholomew GA, Leitner P, Nelson JE (1964) Body temperature, oxygen consumption, and heart rate in three species of flying foxes. *Physiol Zool* 37:179–198.
20. Brown JH, Lasiewski RC (1972) Metabolism of weasels: The cost of being long and thin. *Ecology* 53:939–943.
21. Prothero J (1992) Scaling of bodily proportions in adult terrestrial mammals. *Am J Physiol* 262:R492–R503.
22. Bird RB, Stewart WE, Lightfoot EN (2002) *Transport Phenomena* (Wiley, New York).
23. Kooijman, SALM (2009) *Dynamic Energy Budget Theory for Metabolic Organization* (Cambridge Univ Press, Cambridge, UK).
24. Scholander PF, Hock R, Walters V, Johnson F, Irving L (1950) Heat regulation in some arctic and tropical mammals and birds. *Biol Bull* 99:237–258.
25. Scholander PF, Walters V, Hock R, Irving L (1950) Body insulation of some arctic and tropical mammals and birds. *Biol Bull* 99:225–236.
26. Porter WP, Gates DM (1969) Thermodynamic equilibria of animals with environment. *Ecol Monogr* 39:227–244.
27. Tracy CR, Christian KA (1986) Ecological relations among space, time, and thermal niche axes. *Ecology* 67:609–615.
28. Phillips PK, Heath JE (1992) Heat exchange by the pinna of the African elephant (*Loxodonta africana*). *Comp Biochem Physiol* 101:693–699.
29. McGill BJ, Enquist BJ, Weiher E, Westoby M (2006) Rebuilding community ecology from functional traits. *Trends Ecol Evol* 21:178–185.
30. Kearney M, Porter WP (2006) Ecologists have already started rebuilding community ecology from functional traits. *Trends Ecol Evol* 21:481–482.
31. Meiri S, Dayan T (2003) On the validity of Bergmann's rule. *J Biogeogr* 30:331–351.
32. Freckleton RP, Harvey, PH, Pagel M (2003) Bergmann's rule and body size in mammals. *Am Nat* 161:821–825.
33. Ashton KG, Tracy MC, Queiroz AD (2000) Is Bergmann's rule valid for mammals? *Am Nat* 156:390–415.
34. Blackburn TM, Hawkins BA (2004) Bergmann's rule and the mammal fauna of northern North America. *Ecography* 27:715–724.
35. Mayr E (1956) Geographical character gradients and climatic adaptation. *Evolution (Lawrence, Kans)* 10:105–108.
36. James FC (1970) Geographic size variation in birds and its relationship to climate. *Ecology* 51:365–390.
37. Yom-Tov Y, Nix H (1986) Climatological correlates for body size of five species of Australian mammals. *Biol J Linn Soc* 29:245–262.
38. Natori Y, Porter WP (2007) Japanese serow (*Capricornis crispus*) energetics landscape modeling predicts distribution on Honshu, Japan. *Ecol Appl* 17:1441–1459.
39. Porter WP, Budaraju S, Stewart WE, Ramankutty N (2000) Calculating climate effects on birds and mammals: Impacts on biodiversity, conservation, population parameters, and global community structure. *Am Zool* 40:597–630.
40. McNab BK (1971) On the ecological significance of Bergmann's Rule. *Ecology* 52:845–854.
41. Porter WP, Sabo JL, Tracy CR, Reichman OJ, Ramankutty N (2002) Physiology on a landscape scale: Plant–animal interactions. *Integr Comp Biol* 42:431–453.
42. Porter WP, Vakharia NP, Klousie WD, Duffy D (2006) Po'ouli landscape bioinformatics models predict energetics, behavior, diets, and distribution on Maui. *Integr Comp Biol* 46:1143–1158.
43. Searcy WA (1978) Optimal body sizes at different ambient temperatures: An energetics explanation of Bergmann's Rule. *J Theor Biol* 83:579–593.
44. Kearney M, Porter WP (2009) Mechanistic niche modeling: Combining physiological and spatial data to predict species' ranges. *Ecol Lett* 12:334–350.
45. Chappell MA (1980) Insulation, radiation, and convection in small Arctic mammals. *J Mammal* 61:268–277.
46. Webb DR, McClure PA (1988) Insulation development in an altricial rodent: *Neotoma floridana* Thomas. *Funct Ecol* 2:237–248.
47. Davis LB, Birkebak RC (1975) in *Perspectives in Biophysical Ecology*, eds Gates DM, Schmerl RB (Springer, New York), pp 525–548.
48. Brown JH (1968) Adaptation to environmental temperature in two species of woodrats. *Misc Publ Mus Zool Univ Mich* 135:1–48.
49. Kearney M, Porter WP (2004) Mapping the fundamental niche: Physiology, climate, and the distribution of a nocturnal lizard. *Ecology* 85:3119–3131.
50. Dawson TR (1969) Temperature regulation and evaporative water loss in the brush-tailed possum *Trichosurus vulpecula*. *Comp Biochem Physiol* 28:401–407.
51. Cooper CE, Withers PC (2008) Allometry of evaporative water loss in marsupials: Implications of the effect of ambient relative humidity on the physiology of brushtail possums (*Trichosurus vulpecula*). *J Exp Biol* 211:2759–2766.